Multiple-scattering EXAFS and EXELFS of titanium aluminum alloys

T. Sikora and G. Hug
Laboratoire d'Etudes des Microstructures, CNRS–ONERA, Boîte Postale 72, 92322 Châtillon Cedex, France

M. Jaouen and J. J. Rehr*
Laboratoire de Métallurgie Physique, UMR 6630 du CNRS, Université de Poitiers SP2MI, Bd Marie et Pierre Curie, Téléport 2, Boîte Postale 30179, 86962 Futuroscope Chasseneuil Cedex, France

(Received 25 October 1999; revised manuscript received 30 March 2000)

The extended fine structure of *K* edges of binary intermetallic compounds TiAl, Ti_3Al, and Al_3Ti have been recorded by x-ray absorption spectroscopy (XAS) at the Ti *K* edge and by electron energy-loss spectroscopy (EELS) at the Al *K* edge. The local structure of these titanium aluminum alloys is fully resolved by combining the information retrieved from a spectral analysis of both XAS and EELS data. The data analysis is based on fits to *ab initio* calculations using the real-space multiple scattering code FEFF. It is shown that XAS and EELS can be considered as probes for medium range order studies. This is illustrated for TiAl compounds where it is found that XAS and EELS can be used for site determination of minor elements in ternary dilute alloys. The limitations of this multiple data set approach to fine-structure spectroscopies are briefly discussed.

I. INTRODUCTION

Several ordered intermetallic alloys are currently investigated for aerospace applications at high stress and high temperature. Titanium aluminum based alloys are among the most promising materials for the near future because of their good balance between lightness, strength, and oxidation resistance. In these alloys, the aluminum provides lightness and oxidation resistance, while the transition element provides strength. Among the numerous ordered phases encountered in the Ti-Al phase diagram,[1] we have chosen to study the TiAl, Ti_3Al, and Al_3Ti alloys, which have the simplest crystallographic structure and a wider stability domain. Their structures reflect the ordering of the two atomic species on a simple host lattice, which can be face centered cubic (fcc) or hexagonal compact (hcp). In addition, Ti_3Al and TiAl are the components of the two phase alloys that are under development for aerospace applications. However, both of these compounds suffer from an intrinsic brittleness at low temperature in their single phase form. Many developments are now being undertaken to enhance their mechanical properties by controlling the microstructure and by the addition of several minor elements. Hence, an understanding of the relation of the modification of the physical and mechanical properties to the addition of other elements requires more and more detailed analysis. Nevertheless, upon alloying, changes can be produced at several different scales, ranging from modifications of the microstructure to changes at the atomic scale. In this paper we concentrate on the study of the local atomic order in a homogeneous single phase material. The objective of the present paper is to test the ability of the extended x-ray absorption fine structure (EXAFS) and extended electron energy-loss fine structure (EXELFS) techniques to extract structural information from various alloys and to gauge their inherent limits. Thus in the first step discussed here, we have used only binary compounds in preparation for future applications to ternary compounds.[2]

From these arguments, there is clearly a need for a fine characterization at the local atomic level in these Ti-Al based alloys. Due to their sensitivity to the local atomic environment, the EXAFS and the EXELFS are well-adapted techniques for such studies. In this paper, we first focus on the first near-neighboring shells in Ti-Al alloys by combining the information retrieved from both Ti *K* and Al *K* EXAFS and EXELFS spectra, and show that one can obtain reliable first nearest neighbors (first NN's) distances with these combined data, despite their own different characteristics. Moreover, we also show that one can now retrieve information from shells beyond first-nearest neighbors, by performing an analysis of the high-spatial frequency domain of the EXAFS data using fits to theoretical standards derived from the *ab initio* multiple-scattering code FEFF[3]. Thus EXAFS becomes a medium-range order probe for material science, as will be illustrated here by analysing the TiAl XAS data at the Ti *K* edge up to the eighth nearest neighbors. However, this combined approach of fine-structure spectroscopies, like XAS and EELS, poses some questions. In particular, an experimental EXAFS/EXELFS signal is the incoherent sum of all signals due to each individual absorbing atom in the probed volume, while a given theoretical spectrum is unique to a given absorber atom. Thus the question is, in what sense is a given theoretical spectrum representative of all experimental spectra (e.g., those of individually probed atoms)? One clearly sees that this question is closely related to the disorder existing in the material, a point that remains complicated to handle precisely from a theoretical point of view, without some sort of configurational averaging based on knowledge or assumptions about the nature of the alloy structure. Obviously, the more accurate the information one expects to extract, the more demanding the data quality must be. In the case of EXAFS/EXELFS it means that one must be careful to record XAS and EELS spectra with optimized signal-to-noise ratio over an energy range as wide as possible. Therefore, this approach requires careful sample preparation (annealing, clean surface, ...) prior to performing the

experiments. These conditions are not always easy to fullfil owing to the characteristics of the samples themselves, as will be illustrated with the materials studied here.

The remainder of this paper is outlined as follows. In Sec. II we describe the samples that we have studied and the experimental methods used to obtain the fine-structure data. A brief overview of the data analysis methods is also presented in that section. In Sec. III we give the experimental results and structural informations carried out from their analysis. Finally in Sec. IV, the potential and limitations of the multiple-scattering approach for studies of the intermetallic titanium aluminides are discussed.

II. METHODS

A. Alloy processing and samples preparation

The Ti-Al samples have been processed by the arc-melting technique under argon atmosphere using high-purity starting metals. The main unavoidable impurity was oxygen, which is contained in the titanium with a concentration of about 300 to 400 at. ppm. This is about the best purity available, oxygen being very soluble in titanium. Compared to this fairly high level, extremely few impurities are brought in by the aluminum. The ingots have been subsequently annealed at 1300 °C during 48 h for homogenization, quenched to retain vacancies, and then heat treated again during 100 h at 1000 °C and slowly cooled. In TiAl, the second part of this process results in a precipitation of the impurities (C, N, and O) in small particles.[4] These have a very low-volume fraction ($\leqslant 0.1\%$) and therefore do not contribute significantly to the EXAFS signal. In the EELS experiments, it is easy to select the matrix excluding the precipitates. In Ti_3Al and Al_3Ti no sign of precipitation of a second phase was observed at the scale of the transmission electron microscope.

B. Experimental Methods

Specimens for electron microscopy have been cut with a low-speed diamond saw and thinned by conventional electrochemical and ion-beam milling techniques. EELS spectra have been recorded in a Jeol 4000FX microscope operating at 400 kV and fitted with a Gatan model 666 parallel detection electron spectrometer. The experiments are carried out at 108 K to avoid contamination and to minimize thermal vibrations. (This temperature corresponds to the digital reading on the cold stage of the microscope. The temperature probe is located at a distance from the specimen so the actual temperature of it is not known precisely.) For each spectrum, about ten readouts are recorded in diffraction mode with a low-convergence incident beam ($\leqslant 1.5$ mrad) and a collection aperture of approximately 3 mrad. They are then summed for better statistics. The illuminated area was approximately 2 μm in diameter with thicknesses below 100 nm. The integration time on the photodiode array (PDA) lies between 25 s and 50 s, depending on the probed alloy. The probe current was kept sufficiently low ($\leqslant 400$ nA) to minimize irradiation effects and great care was taken to avoid specimen drift. The actual experimental resolution, measured as the half-width of the zero loss peak was found to be 1.5 eV. Each spectrum is corrected for the defects of the PDA. Dark counts are recorded with 10 times more readouts than the raw data to cancel the statistical noise and to keep only the systematic noise. Once divided by 10, this dark-count signal is subtracted from the raw data. Then, the resulting spectrum is corrected for channel-to-channel gain variation by dividing it by a spectrum acquired with uniform illumination, which is previously corrected for dark counts. A low-loss spectrum is also recorded with the same illuminated area. After extraction of the background with a standard power-law function, plural scattering contributions are removed by using the standard Fourier ratio deconvolution procedure.[5] All these treatments are performed within the GATAN EL/P program.

Because of their brittleness, intermetallic specimens cannot be thinned enough to reach x-ray transparency to perform XAS experiments in transmission mode. Consequently, small square samples of 20 mm^2 and 5 mm thick have been prepared for experiments in the conversion electron yield mode (CEEXAFS).[6] Prior to the experiments, their surfaces have been mechanically polished down to 5 μm diamond grain to remove surface damage. Ti *K* edge XAS electron yield spectra were recorded on beam-line D44 of the 1.3 GeV positron storage ring DCI at LURE using a two-crystal type Si (111) monochromator (0.7 eV resolution) equipped with mirrors for harmonics rejection. To reduce thermal disorder, the XAS data were collected at 77 K using a CEEXAFS device working at the liquid-nitrogen temperature under helium flow.[7] The energy step was 2 eV and the acquisition time per data point 2 s.

To conclude this section, we discuss the reasons underlying our choice of using EELS at the Al *K* edge and XAS at the Ti *K* edge to study Ti-Al intermetallics, as well as their consequences. Indeed, we have previously shown[8,9] that it is now feasible to record EELS spectra in the 4–7 keV energy range. In this range, the EELS signal-to-noise ratio for high values of the wave vector *k* is not as good as for XAS. Since a reliable multiple-scattering analysis requires as wide as possible a *k* range, this favors the XAS technique, which also has the advantage of being easier to use than EELS and offers better energy resolution. Unfortunately, except for the YB_{66} monochromator[10] at SSRL (Stanford, CA), available monochromators at synchrotron facilities for probing the Al *K* edge are quartz, which have intrinsic absorption at the Si *K* edge. Clearly, the EELS technique does not suffer such a limitation, which is why we have employed it for Al *K* edge studies. The use of two different techniques for probing the Al *K* and Ti *K* edges of the Ti-Al alloys introduces some additional limitations. For a given composition, EELS- and XAS-probed samples have undergone different treatments (electrochemical and ion-beam milling on one side, mechanical polishing on the other) and the temperatures of the measurements are different. Furthermore, the CEEXAFS technique is very surface sensitive. Even if the depth probed in electron yield mode is not known precisely,[11] it can be roughly estimated using a semiphenomenological model[12–14] to range between 40 and 70 nm, depending on the Ti concentration for Ti_3Al and Al_3Ti, respectively. From all these considerations, it turns out that one cannot expect to find ''*a priori*'' equal Debye-Waller factors for Ti and Al heteropairs, as must be the case when one probes both atomic species using the same sample and same experimental conditions.

C. Methods of Analysis

Provided the collection angle of the spectrometer is small enough to be consistent with the dipole approximation, it has been established that the EXELFS signal contains the same structure information as EXAFS,[15] and thus that they can be both expressed within the same theoretical framework. The principle of the EXAFS/EXELFS relies on the behavior inside a condensed material of an electron ejected from a central atom either after an x-ray photon has been absorbed (XAS) or from the inelastic scattering of a fast electron (EELS). However, due to the different inelastic cross sections for photons and fast electrons, the energy dependence of pre-edge and post-edge background is different, and one must correct for EELS spectra accordingly before analysis.[16] If one takes this correction into account especially when studying low Z materials,[17] we have found[18] that it is less important when working in the 2 keV range (Al K edge: 1.56 keV). We do not summarize here the basis of the EXAFS/EXELFS theory, since it is now well established and well documented,[19–23] but only describe the various tools we have used for data analysis: once the pre-edge has been subtracted with a linear (XAS) or power law[5] (EELS), the post-edge background is extracted using the AUTOBK code,[24] which has the advantage of providing a well-defined atomic absorption background and removing low-frequency oscillations that may be considered as an atomic XAFS (AXAFS).[25] The obtained $\chi(k)$ EXAFS/EXELFS function is then adjusted to the related structural model generated by FEFF for both single scattering and multiple scattering (MS) paths using the FEFFIT(Ref. 26) fitting code, which is fully compatible with FEFF. Indeed, to perform an EXAFS/EXELFS analysis, one needs accurate backscattering parameters, and the FEFF code has been found to be one of the best for such a purpose.[27] The FEFF code also includes important corrections for self-energy and core-hole effects, the self-energy being a crucial ingredient in *ab initio* fine-structure calculations[28]. In all cases we have used the analytical Hedin-Lundquist self-energy model[29] implemented in FEFF. The FEFFIT program is very flexible, and uncertainties and errors are handled in a sophisticated way, based on standard error analysis theory. Furthermore, to avoid spurious structures due to the Fourier backtransform, fittings are performed in r space using both imaginary and real parts of the Fourier transforms. For all spectra analyzed here, the $\chi(k)$ EXAFS/EXELFS function was k^2 weighted before being Fourier transformed using a Hanning window. Moreover we use all the possibilities offered by FEFF for analyzing higher order MS contributions in Ti-Al EXAFS/EXELFS spectra. MS simulations of experimental data also address a severe problem concerning the proper handling of disorder for MS paths. Even though its utilization may be questionable for structures other than cubic, we have used the optional correlated Debye-Waller model[30] included in FEFF to treat the thermal part of MS paths disorder.

For all simulations presented hereafter, the FEFF calculations are performed starting from the known crystallographic structure of a given alloy. The corresponding experimental data are then fitted to these theoretical spectra that are used as input to FEFFIT. Throughout this paper, the coordination numbers have been fixed to the nominal composition of the samples. Thus the only parameters that are adjusted are the first NN distances, the Debye-Waller (DW) factors or Debye temperature Θ_D, the energy origin E_0 for the interstitial muffin-tin potential, and a damping factor Γ to take into account the energy resolution and local disorder in potentials. The global amplitude reduction factor S_0^2 ascribed to the possibility of multiple electron excitations at the absorbing atom is fixed at the values determined[18] from the analysis of bulk titanium (XAS, $S_0^2=0.72$) and aluminum (EELS, $S_0^2=0.78$).

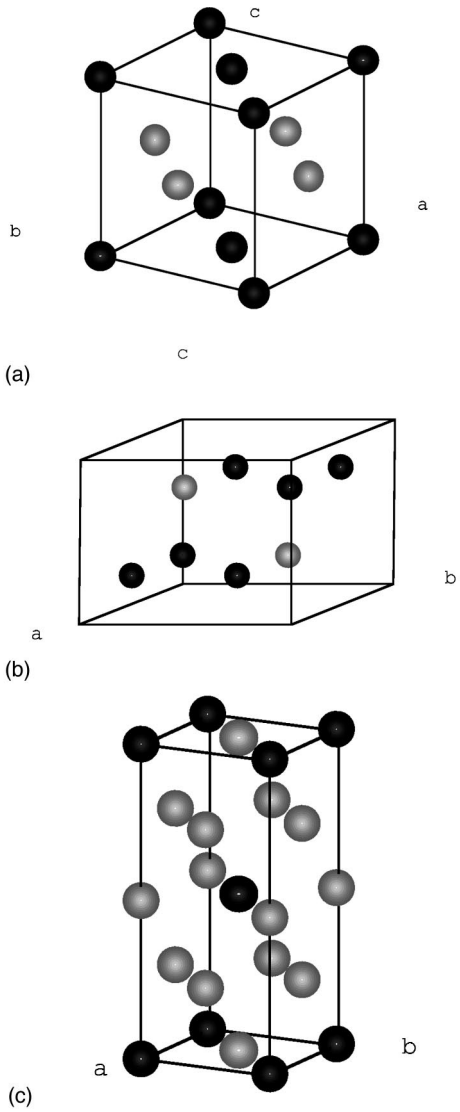

FIG. 1. Unit cells of TiAl (a), Ti_3Al (b), and Al_3Ti (c) alloys. Ti atoms are in black and Al atoms in gray.

III. EXPERIMENTAL RESULTS

A. TiAl alloy

The TiAl intermetallic compound crystallizes under the $L1_0$ structure (space group $P4/mmm$), which is based on the ordering of the Al and Ti atoms on the fcc lattice. It consists of alternate pure (001) planes of aluminum and titanium (Fig. 1). In the Ti-Al phase diagram, two phases are present at the equiatomic composition: the hexagonal α_2 phase (Ti_3Al) and the γ phase (TiAl). For this reason the alloys

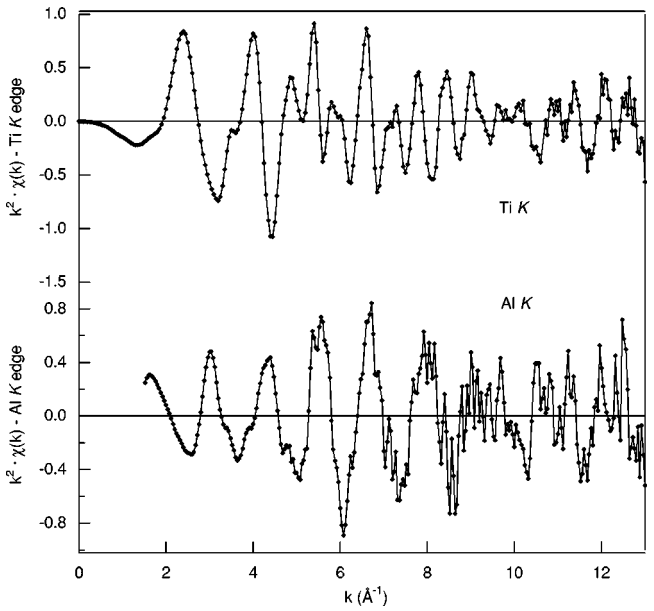

FIG. 2. TiAl alloy Al K (EELS: bottom) and Ti K (XAS: top) $k^2 \cdot \chi(k)$ spectra.

studied here are slightly aluminum enriched, in order to belong to a single phase domain. The actual composition measured with a Castaing microprobe is $Ti_{46}Al_{54}$ and the lattice parameters measured by x-ray diffraction (XRD) are $a = 3.991$ Å and $c = 4.081$ Å.

The raw $k^2 \cdot \chi(k)$ functions related to Al K and Ti K edges are plotted in Fig. 2. The first noticeable point is the striking weakness of the Ti K EXAFS oscillations. We have shown in a previous paper[9] that this particularity is intrinsic to the TiAl alloy. This is due to the fact that the difference between Ti and Al backscattering phase shifts is nearly constant and equal to about 3 rad in the (5 $Å^{-1}$ − 12 $Å^{-1}$) k-space range so that first NN's Al and Ti EXAFS contributions are approximately out of phase. The second remarkable point is that the Al K EELS data become rather noisy beyond about 9.5 $Å^{-1}$ and thus cannot be used to retrieve reliable information from their analysis. We will return to these points later, but they illustrate some of the experimental difficulties encountered when probing titanium aluminides on a wide k range.

1. Ti K edge

Figure 3 shows the XAFS radial distribution function (RDF) modulus obtained after Fourier transform of the spectrum displayed in Fig. 2 over the k-space range (3.3 − 11.8 $Å^{-1}$). One should remark at the unusually strong peak at about 5 Å compared to the first one at about 2 Å . In apparent distances, the intense peak at 5 Å corresponds to the fourth NN's in the $L1_0$ structure, and the one at 2 Å corresponds to the Ti and Al first NN's that are, from the crystallography, separated by $\Delta r \approx 0.026$ Å. This low distance aside, the fact noted above that Ti and Al contributions are nearly out-of-phase,[9] explains the weakness of the first peak of the RDF. Nevertheless, even if not entirely resolved, one can clearly observe the splitting of this first peak in the two components associated to the first NN's Ti and Al backscatters. However, one cannot expect to separate these two contributions by filtering: they must instead be treated simultaneously in a fitting procedure. The best fit corresponding to the first NN's contributions is shown in Fig. 4, and the results are summarized in Table I: the adjusted global param-

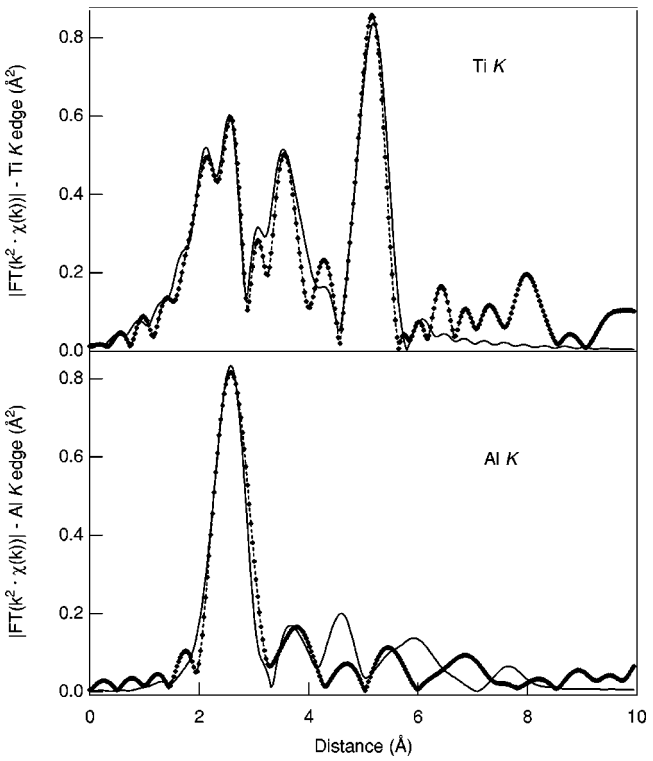

FIG. 3. Ti K (XAS: top) and Al K (EELS: bottom) experimental (dotted curves with symbols) and fitted (solid curves) FMS theoretical RDF's for TiAl.

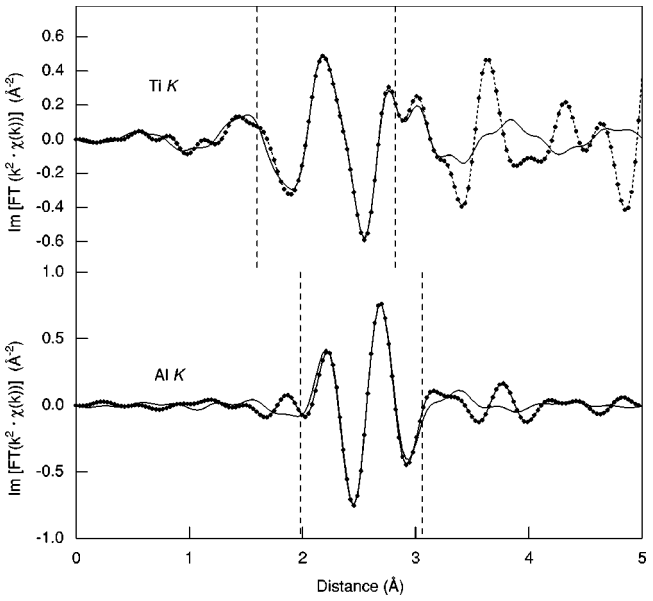

FIG. 4. Fits to the Ti K EXAFS (top) and AlK EXELFS (bottom) $\chi(R)$ in TiAl for the first NN contributions (imaginary part). The dotted curves with symbols show the experimental data; the solid curves show the fits to the experimental data. The fit range $[R_{min}, R_{max}]$ is indicated by dashed lines. Fits results are given in Tables I and II, respectively.

TABLE I. Results of the $Ti_{46}Al_{54}$ EXAFS fit at Ti K edge; $S_0^2 = 0.72$, $\Gamma = 0.8$ eV.

N	Distance (Å)	σ^2 (Å^2)
3.68 Ti	2.81 ± 0.01	0.0021 ± 0.0005
8.32 Al	2.82 ± 0.01	0.0035 ± 0.0005

TABLE II. Results of the $Ti_{46}Al_{54}$ EXELFS fit at Al K edge; $S_0^2 = 0.78$, $\Gamma = 1.0$ eV.

N	Distance (Å)	σ^2 (Å^2)
4.32 Al	2.80 ± 0.01	0.0027 ± 0.0005
7.68 Ti	2.82 ± 0.01	0.0073 ± 0.0005

eters are found to be $E_0 = (0.0 \pm 0.5)$ eV and $\Gamma = (0.8 \pm 0.1)$ eV. Such a fair fit suggests that the local structure is more cubic than quadratic, since the local c/a ratio obtained is slightly smaller than that deduced from XRD measurements, although it still lies within the error bars ($c/a = 1.01 \pm 0.01$ instead of 1.022 ± 0.003 for XRD). Notice also that the disorder is found to be higher for heteropairs than for homopairs, a behavior that has been previously reported when analyzing the EXAFS signal as a function of the temperature, and has been assumed to be a precursor of a phonon soft mode.[9]

To go beyond the first neighboring shell, we then performed a MS calculation using a larger cluster of radius 5.59 Å, which involves 55 atoms (8 coordination shells). By selecting only those paths whose amplitude has a weight greater than 4% of the largest ones (e.g., the two first coordination shells: 100%), we obtained a theoretical spectrum involving 38 different scattering paths. All these paths where used as input to the fitting program FEFFIT. The two first shells distances, the DW factors as well as the global parameters E_0 and Γ, were fixed at the values obtained previously (Table I). The distances for the higher-order shells were kept equal to the crystallographic ones and the only adjustable parameter was a global DW factor σ_g^2 for all paths but the two first ones. With this simple model, we obtained a good fit of the experimental data up to 6 Å as shown in Fig. 3. The value found for the DW was $\sigma_g^2 = (0.0137 \pm 0.0025)$. The very good agreement between experiment and theory is worth noticing for the particularly intense fourth peak of the RDF located at 5 Å that was discussed previously. From the examination of the MS data calculated by FEFF, one can easily correlate this peculiar feature of the Ti K RDF to the structure of the TiAl alloy. In the fcc based $L1_0$ structure, the first NN's and fourth NN's are aligned along $\langle 110 \rangle$ directions. Among the large amount of paths contributing to the fourth peak of the RDF, the most important ones are the threefold paths showing strong focusing effects on the fourth shell through either aluminum ($\langle 011]$ directions : Ti-Al-Ti) or titanium ($\langle 110]$ directions: Ti-Ti-Ti) second NN's atoms. These paths involve only backward and forward scattering whose weight is known to be the strongest. The total contribution of the Ti-Al-Ti paths is nearly two times (degeneracy: 16, weight: 53%) larger than one of the Ti-Ti-Ti paths (degeneracy: 8, weight: 31.4%). This example shows clearly how a MS analysis, when feasible, becomes a powerful tool to study higher-order correlation functions such as the three and four bodies ones we have shown to be important to interpret the Ti K edge XAFS data. In that sense, EXAFS can be viewed as a method for probing the medium range order of materials.

2. Al K edge

Figure 3 shows the RDF modulus obtained once the Al K $\chi(k)$ spectrum displayed in Fig. 2 has been Fourier transformed in the k-space range (3.3 Å^{-1}–9.5 Å^{-1}). It should be noticed that the overall shape of this RDF is more typical than that obtained at the Ti K edge (Fig. 3). The simulation of the real and imaginary parts of the RDF that corresponds to the two first coordination shells was performed by adjusting six parameters (two distances, two DW factors, E_0 and Γ). The best fit is shown in Fig. 4 and results are gathered in Table II, the global parameters being found to be $E_0 = (9.0 \pm 0.5)$ eV, $\Gamma = (1.0 \pm 0.1)$ eV. One can note that the Al–Ti distances are equal to the ones obtained at the Ti K edge, a satisfactory result despite the differences between the XAS and EELS techniques. Obviously, this is not the case for DW factors as discussed above (different samples and different temperatures of measurements). However, we observe again that the disorder is higher in mixed Ti-Al planes than in pure Al ones (or pure Ti planes at the Ti K edge). Such a result could be ascribed to the fact that bonds are stronger for homopairs than for heteropairs in γ-TiAl. Such a behavior would play a significant role in the mechanical properties of this alloy.[31]

We have not been able to perform a trustworthy MS fit for the EELS Al K edge data, since it would have required a number of parameters far exceeding the number of independent data points given by the Shannon theorem.[34] Indeed, since the alloy composition is out of stoichiometry, there are a significant number of Al atoms on the Ti sites, and this requires us to take into account two different sites for Al atoms and hence a large number of parameters. The too short k range available illustrates the point previously mentioned that to perform a reliable MS analysis, it is necessary to acquire experimental spectra over a wide k range with a sufficiently high-signal-to-noise ratio. Nevertheless, we wanted to know if there exists a focussing effect at the Al K edge that would give rise to an intense peak in the RDF, as observed at 5 Å at the Ti K edge. For this purpose, we performed a purely theoretical MS calculation, running FEFF for the cluster used for the Ti K-edge MS fitting but with a central aluminum absorbing atom. Furthermore, we imposed for the two first coordination shells the set of parameters reported in Table II (as well as for the global parameters E_0 and Γ) and for all other shells the global DW factor obtained from the Ti K MS fit. The FEFF calculated $\chi(k)$ function was then Fourier transformed in the same k range used for experimental Ti K-edge (k) data. This Fourier transform is plotted in Fig. 3. It is obviously not surprising that this theoretical RDF does not match the experimental one for large distances; but the most interesting point is that both experimental and theoretical RDF's do not show any intense peak in the vicinity of 5 Å. This result is of great importance, since it implies that we can use the XAS or EELS spectrometry as a site selective technique in γ-TiAl intermetallic alloys. In that sense it is very competitive with the ALCHEMI technique,[32] which is used for site determination of minor

addition elements but requires the existence of an alternation of two planes of different compositions in the material. We actually used the RDF fingerprints to study the site occupancy of solute elements in ternary dilute $(TiAl)_{97}X_3$ (X = Mn, Nb, Cr) alloys.[2] To conclude, it should be outlined that the difference observed at Al K and Ti K RDF's only reflects the different scattering powers that are nicely reproduced by the FEFF code, of Al and Ti atoms in the $L1_0$ structure.

B. Ti_3Al alloy

The Ti_3Al alloy crystallizes in a hexagonal DO_{19} structure ($P6_3/mmc$), which is an ordered superstructure on the α-Ti hcp lattice. The composition of basal planes is Ti_3Al with an AB stacking. Along a direction normal to prismatic planes (direction $\langle 11\bar{2}0\rangle$), the structure can be viewed as composed of an alternate stacking of pure Ti and TiAl planes (Fig. 1). Its lattice parameters measured by XRD are $a=5.782$ Å and $c=4.629$ Å.

1. Ti K edge

The XAS data related to this alloy have been recorded at room temperature. From the crystallographic structure of this compound, the first peak of the RDF includes contributions from the four first coordination shells. These four shells correspond to the 12 first NN's in the hcp packing that are Ti-Al and Ti-Ti distances in the basal plane and Ti-Al and Ti-Ti distances that have a component along the **c** axis. Therefore the EXAFS analysis requires to adjust a large number of parameters (theoretically 14), exceeding the number of independent points avalaible in the data set [k-space range: (4.5 $Å^{-1}$–11 $Å^{-1}$)]. Thus to reduce the number of adjustable parameters and obtain a trustworthy fit, we fixed the energy origin E_0 to zero for all shells while the global amplitude reduction and damping factors were set equal to the values deduced from the analysis performed at the Ti K edge for the TiAl alloy (Sec. III A 1). Therefore we only adjust four parameters: one distance and one DW factor for both first and second shells that are constituted of 2 Al + 4 Ti in each case. We obtained a very good fit of the first peak of the imaginary part of the RDF, as is shown in Fig. 5, the values of the related parameter are summarized in Table III. Although the fitted distances are in excellent agreement with the crystallographic ones, we note that the c/a ratio value here is also smaller than the one obtained from XRD measurements.

As for the TiAl alloy, we tried to perform a MS simulation of the data using a larger cluster (radius 7.154 Å 19 coordination shells). The fitting range was extended to (1.72 Å–11.5 Å) in the r space, a range that allows to adjust 22 parameters. Since the theoretical spectrum includes 76 different scattering paths (19 twofold, 36 threefold, 21 fourfold), one must use a strategy to limit as much as possible the number of adjustable parameters. Therefore, we have fixed the parameters related to the first four coordination shells to the values obtained from the previous analysis of the first peak of the RDF (Table III) because they represent the main contribution of the EXAFS signal. Obviously, it must be the same for the three global parameters that are S_0^2, Γ, and E_0. Thus we only search for the DW factors for all other shells using the correlated Debye model implemented in FEFF. The

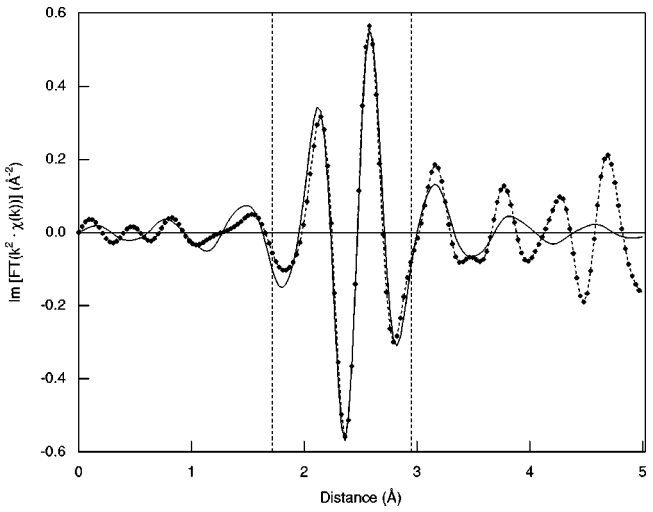

FIG. 5. Fit to the TiK EXAFS $\chi(R)$ for Ti_3Al (imaginary part). The dotted curve with symbols shows the experimental data; the solid curve shows the fit to the experimental data. The fit range $[R_{min}, R_{max}]$ is indicated by vertical-dashed lines. Fit results are given in Table III.

Debye temperature we obtain is $\Theta_D=300$ K. We have not found in the literature its value for the Ti_3Al alloy, but such a value seems to be too low when compared to those of the pure metals Al and Ti ($\Theta_D^{Ti}=380$ K, $\Theta_D^{Al}=394$ K). Furthermore, looking at the Fourier transform of this fit displayed in Fig. 6, one can note that the agreement with the experiment is poor, especially between 3 and 4.2 Å . A more detailed analysis shows that the main contribution in that r range comes from the fifth coordination shell (6 Ti at 4.06 Å) and it seems that they are located at a too short apparent distance (dashed line in Fig. 6). It means that the local structure is rather disturbed beyond the first four coordination shells. An accurate fit of the data would require to adjust a DW factor for each scattering path and thus a huge number of fitting parameters. The structure being complex (if the peaks located at 4.5 and 5.5 Å are qualitatively well reproduced, they mainly include multiple scattering contributions), the search for a reliable simulation becomes unrealistic.

This example illustrates the limits of a multiple-scattering analysis on both experimental and theoretical points of view. However, it must be mentioned that some of the difficulties encountered during the ''all shells'' simulation of this data set might come from the detection mode we used (CEEX-AFS). As noted before, the measured signal is very surface sensitive[11] and it is likely that the post annealing treatment was unsatisfactory to remove all the damage induced during the mechanical polishing of the sample.

TABLE III. Results of the Ti_3Al EXAFS fit at Ti K edge; $S_0^2=0.72$, $\Gamma=0.8$ eV.

N	Distance (Å)	σ^2 ($Å^2$)
2 Al	2.87±0.01	0.004±0.001
4 Ti	2.87±0.01	0.008±0.001
2 Al	2.90±0.01	0.004±0.001
4 Ti	2.90±0.01	0.008±0.001

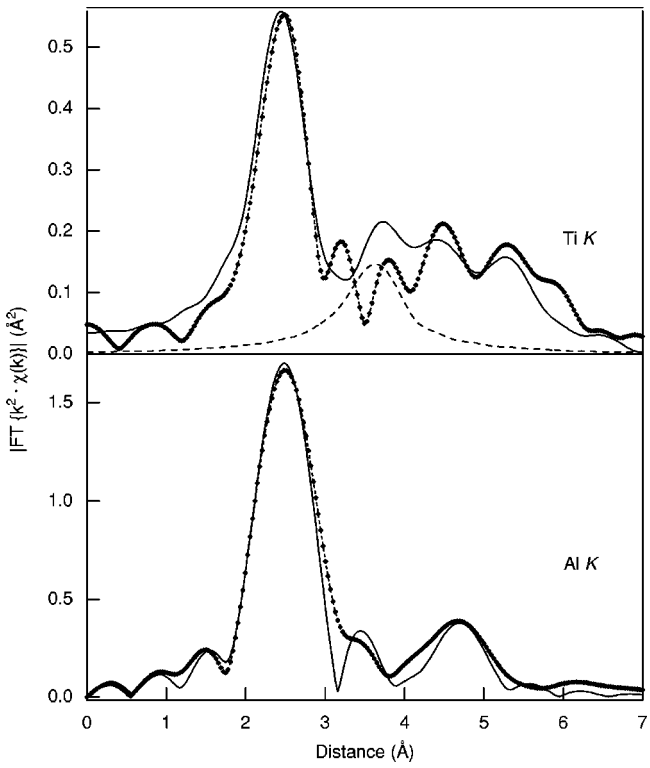

FIG. 6. Ti *K* (XAS: top) and Al *K* (EELS: bottom) experimental (dotted curves with symbols) and fitted (solid curve) FMS theoretical RDF for Ti_3Al. The dashed line shows the fifth shell contribution (see the text).

2. Al K edge

Paradoxically, the ''all shells'' analysis of the Al *K*-edge EELS data turned out to be much easier, as can be observed in Fig. 6. This fit was performed on an 8-shells cluster (radius 5.775 Å). The Fourier transform was performed in the *k* range (3 $Å^{-1}$–8 $Å^{-1}$) and the theoretical adjustment in the *r* range (1.84 Å–5.89 Å), leading to 14 independent points. In fact, the fit only needs a few number of parameters. Indeed, we fixed the two global factors S_0^2 (0.78) and Γ (1 eV) at the values obtained from the TiAl Al *K*-edge analysis (Sec. III A 2). We then adjusted a global energy origin factor E_0, found to be 4 eV, and a Debye temperature using the correlated Debye model (the EELS experiment was performed at 114 K). We obtain $\Theta_D = 245$ K, a value that also seems to be too low and furthermore different from the one obtained from the Ti *K*-edge analysis, a point that we will address later in the discussion. The values of the structural parameters related to the two first coordination shells are given in Table IV. One notes that the Ti-Al pair's DW factors are different at both edges (Table III), but it is most probably due to the fact that the probed samples and the temperature of the measurements are different.

TABLE IV. Results of the Ti_3Al EXELFS fit at Al *K* edge; $S_0^2 = 0.78$, $\Gamma = 1.0$ eV.

N	Distance (Å)	σ^2 ($Å^2$)
6 Ti	2.856	0.011 ± 0.001
6 Ti	2.887	0.011 ± 0.001

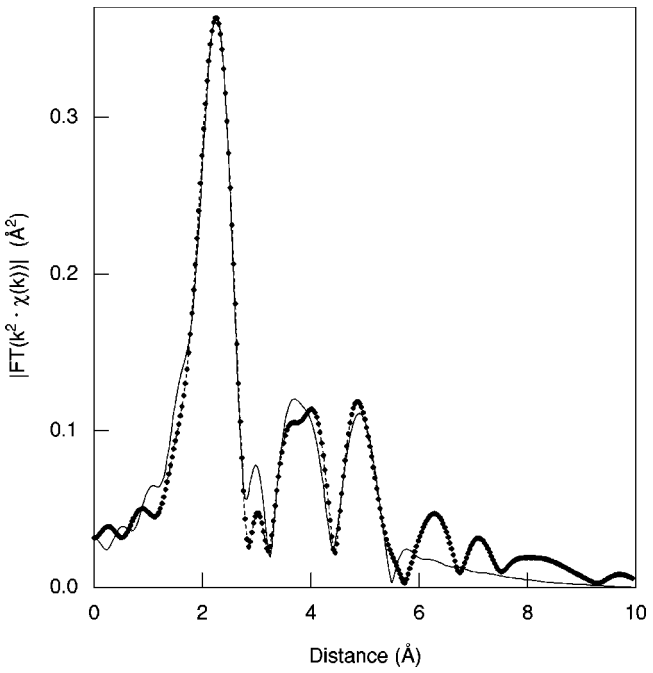

FIG. 7. Ti *K* (XAS) experimental (dotted curve with symbols) and fitted (solid curve) FMS theoretical RDF for Al_3Ti.

C. Al_3Ti alloy

The Al_3Ti alloy crystallizes in the DO_{22} structure (space group $I4/mmm$) which is ordered on the fcc lattice. This structure presents three different sites labeled (a), (b), and (d) in the Wyckoff notations, which are occupied by Ti, Al, and Al_2 atoms, respectively. The DO_{22} structure can be described from the $L1_2$ structure in which a periodic modulation of conservative antiphases[33] is introduced along the **c** axis. The lattice parameters measured by XRD are $a = 3.848$ Å and $c = 8.596$ Å.

1. Ti K edge

As for the Ti_3Al alloy, the XAS data have been recorded at room temperature in conversion electron yield mode. The Fourier transform is thus restricted to the *k* range (2 $Å^{-1}$–8.25 $Å^{-1}$) which corresponds, for a fit performed in the *r* range (1.71 Å–2.94 Å), to six independent points. Here also, we fix the values of the two global parameters S_0^2 and Γ to those obtained from the fit of the TiAl Ti *K*-edge data (Sec. III A 1). By noticing the asymetrical shape (non-Gaussian) of the first peak of the RDF (Fig. 7), we tried a fit using a cumulant expansion up to the third order. Indeed, if the distribution is asymmetric, then one can either use multiple Gaussian shells that are offset by a small distance variation δr or describe the nearest-neighboring shells by a single distribution that includes a cumulant expansion whose order is higher than the second one. In the latter case, the number of adjustable parameters is theoretically less than in the former case. However, for the studied alloy, we know from the crystallography that the two shells we have to consider are well separated (from about 0.16 Å) so that their description in terms of a single asymmetric distribution becomes unphysical. Thus we only search for three parameters: a global energy shift E_0 (3.12 eV in the present case), one DW

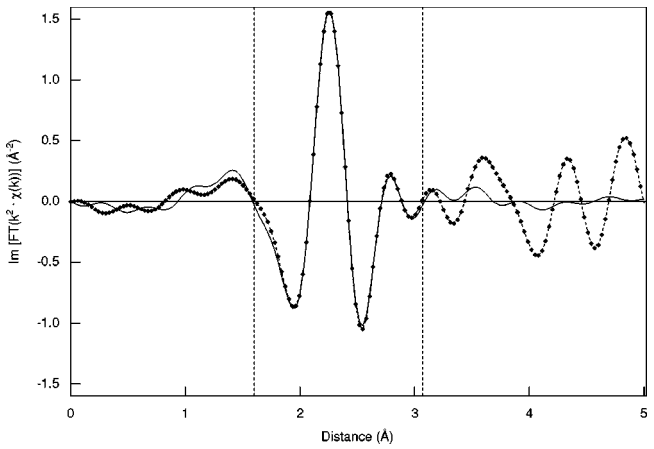

FIG. 8. Fit to EXAFS $\chi(R)$ for Al_3Ti. The dotted curve with symbols shows the experimental data; the solid curve shows the fit to the experimental data. The fit range [R_{min} and R_{max}] is indicated by vertical-dashed lines. Fit results are given in Table V.

factor and one third order cumulant, the distances being fixed at their crystallographic values. The resulting fit of the imaginary part, the first peak of the RDF, is shown in Fig. 8 and the related fitted values are given in Table V. The overall agreement with the experimental data is quite satisfactory, especially on the low side of the fitted *r* range that was badly reproduced in a model that only includes a cumulant expansion up to the second order (not shown here). Such a result suggests that each Al_1 and Al_2 site is characterized by a wide distribution of distances with respect to a Ti atom rather than by a single well-defined distance. This example outlines how it is important to record the data over a wide *k* range since the number of parameters needed to perform an analysis of asymmetric distributions increases when the shells to consider are widely separated as in the case of the Al_3Ti alloy.

As in previous cases, we then performed a MS analysis of the experimental data using a larger cluster (radius 5.77 Å) which corresponds to 25 different scattering paths. The distances were fixed to their crystallographic values while the set of parameters related to the two first shells, as well as the global factors, were those deduced from the analysis described above (Table V). In the fitting procedure, we only adjust a DW factor for each of the five single-scattering paths belonging to the considered cluster and a Debye temperature for higher-order scattering paths (3 legs and 4 legs paths). As it can be seen in Fig. 7, the fitted RDF is in good agreement with the experimental one. Even if the so obtained Debye temperature ($\Theta_D = 345$ K) seems to be more realistic than the one found from the MS analysis of the Ti_3Al alloy (Sec. III B), it should not be considered a reliable result. This Debye temperature is likely to be ascribed to an insufficient number of available independent points in the data set to perform a fit of each MS path rather than the actual Debye temperature of the alloy.

TABLE V. Results of the Al_3Ti EXAFS fit at Ti *K* edge using a cumulant expansion up to the third order; $S_0^2 = 0.72$, $\Gamma = 0.8$ eV.

N	Distance (Å)	σ^2 (Å^2)	σ^3 (Å^3)
4 Al_1	2.727	0.0029 ± 0.0007	0.0009 ± 0.0002
8 Al_2	2.885	0.0029 ± 0.0007	0.0009 ± 0.0002

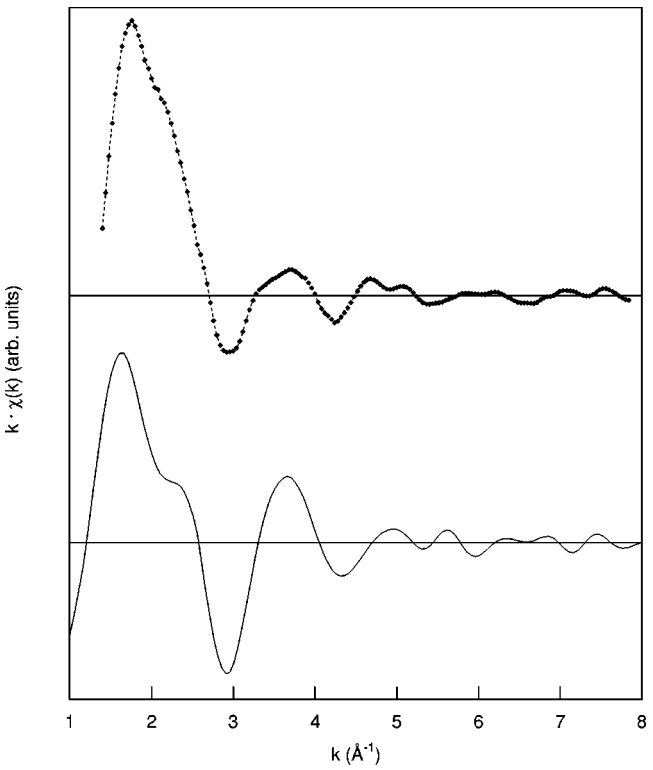

FIG. 9. Comparison between experimental and theoretical FMS $\chi(k)$ spectra for Al_3Ti (Al *K* edge).

2. Al K edge

As mentioned above, there exists in the DO_{22} structure two different aluminum sites corresponding to different atomic environments: (Al_1: 4 Ti at 2.727 Å + 8 Al_2 at 2.885 Å; Al_2: 4 Al_2 at 2.727 Å, and 4 Al_1 + 4 Ti at 2.885 Å). It is therefore impossible to perform a reliable analysis of the EXELFS signal at the Al *K* edge. Indeed, in that case any realistic simulation of the experimental data would require the adjustment of a number of parameters far exceeding the number of independent points in the data, the *k* range being limited here to about 8 Å^{-1}. Therefore, we perform two FEFF calculations, one per aluminum site, using the set of parameters deduced from the Ti *K*-edge analysis. Once weighted by the occupation ratio of each site (Al_1: 1, Al_2: 2) in the unit cell, these two spectra are summed up to obtain the theoretical EXELFS signal (see Fig. 9). They are found to be nearly out of phase beyond k $\approx$ 4 Å^{-1} so that the signal is strongly damped above that *k* value and makes it very difficult to obtain a reliable fit of the experiment data. Even if all experimental fine structures are qualitatively reproduced by the FEFF calculations (Fig. 9), one can thus observe that the predicted theoretical *k* periodicity of the signal is larger than the experimental one. It is very likely to be connected to the fact that the theoretical full multiple scattering calculations performed for each aluminum site do include asymmetric distributions of distances, except for the first titanium nearest-neighboring shell.

IV. DISCUSSION

From all the results presented above, we wish to comment on the following points. First, we have shown that the multiple-scattering approach gives a very accurate description of the near-neighbor surroundings in titanium aluminides alloys, at both Ti *K* and Al *K* edges. Indeed, from the analysis of the first RDF peak, we always found that the values of the first NN's distances are consistent at both *K* edges and also, within the error bars, with the crystallographic data of these compounds. Second, we would like to emphasize both the advantages and limitations of combining the XAS and EELS methods to study aluminum-based intermetallic compounds. Although it has been known for a long time[15] that EELS and XAS signals contain the same kind of information, up to now it appears that no one has made simultaneously use of EELS and XAS to study a given material. We have demonstrated here the potentialities of such an approach. On the one hand, it allows us to improve the accuracy of heteropair Ti-Al distances. However, on the other hand, we have pointed out the difficulties of comparing the DW factors obtained from the analysis of the XAS and EELS spectra related to the same alloy. It comes from the differences existing between these two techniques and from the particularities of the analyzed samples here. To perform accurate EELS measurements, we need a sample thin enough to reach electron transparency, whereas for XAS spectra collection we are compelled, owing to the brittleness of titanium aluminides, to use the TEY mode, which is highly-surface sensitive. It is therefore not surprising to find different DW factors for heteropairs when fitting the Ti *K* and Al *K* data recorded on the same alloy, the temperatures of the experiments being different. Third, we have proved that it is now feasible to go beyond the traditional and straightforward first shell analysis. To obtain useful structural information from higher-order shells, it is necessary to use a more complex approach, since their extraction is generally complicated by the photoelectron multiple-scattering processes. Therefore the analysis must be done with a more sophisticated method to take into account these multiple-scattering effects. Such a goal can be achieved by using the FEFF and FEFFIT codes, as has been clearly illustrated with the MS analysis performed at the Ti *K* edge (Sec. III A 1) of the TiAl compound. In particular, we have been able to explain the large focusing effect of the first NN's onto the fourth NN's, which is responsible for a very intense peak in the RDF at about 5 Å as well as the weakness of the first peak due to destructive interferences. This feature is characteristic of the Ti site and not of the Al one, and thus can be used as a fingerprint to determine the site occupancy of solute elements[2] that are added to improve the mechanical properties of the TiAl alloys. All these results give an accurate description[35] of the γ-TiAl structure down to the atomic scale.

However, from an experimental point of view, it is important to record high-quality spectra over a wide *k* range to make a useful comparison with theoretical calculations that include MS contributions. At the present time, this condition is not generally fulfilled for EELS, the data being generally too noisy beyond about 8–9 $Å^{-1}$. A too limited *k* range of the data set can even make the analysis impossible for material with a complex structure. It has been illustrated with the Al_3Ti alloy, which Al *K*-edge FMS analysis (Sec. III C 2) would be required to adjust a too large number of free structural parameters due to the existence of two different Al sites. In such an extreme case, we have shown that it was even impossible to fit the first NN's distances despite the fact that heteropair distances have been determined from the Ti *K*-edge analysis. From a theoretical point of view, we have also shown that the main bottleneck of any MS analysis is in the determination of the DW factors of the MS paths. Theoretically, one has to fit one DW factor per scattering path, so that the problem becomes inextricable when the selected cluster size is large and/or the structure complex. In practice, the problem becomes feasible if one uses only a limited number of parameters to describe the thermal and static disorders existing in the probed material. This is partly achieved by using the correlated Debye model implemented in FEFF. We found that this model mimics correctly the disorder in cubic structures like TiAl (Sec. III A 1) and Al_3Ti (Sec. III C 1), even though the obtained Debye temperatures do not seem to be fully realistic. Obviously, it does not work so well for an hexagonal structure like DO_{19}. Thus a key point for the theory for future use of the MS theory as a practical tool for structural studies of materials, is to take into account the MS DW factors with a minimum number of input parameters. This task is currently in progress.[36,37]

V. CONCLUSIONS

By combining XAS and EELS spectroscopies, we have presented in this paper a detailed analysis of the local structure existing in the three defined compounds of the Ti-Al phase diagram: TiAl, Ti_3Al, and Al_3Ti. The ''*ab initio*'' FEFF calculations, linked with the FEFFIT fitting code, have been shown to be very efficient for determining accurate structural informations, including both near-neighbor and higher-shell distances. The consistency[9] between the XAS and EELS techniques has also been attested for first near-neighbor distances, but we have also shown how difficult it is to compare heteropair DW factors due to the experimental specificity of each of these spectroscopies.

We have demonstrated that one can go beyond the usual first shell analysis by using all the potentialities of the FEFF approach that makes now tractable a multiple-scattering analysis of the fine structures. The usefulness to extract all the information contained in fine-structure spectra is clearly illustrated in the case of the TiAl alloy at the Ti *K* edge. From the MS analysis, we have been able to resolve entirely the structure up to 6 Å, i.e., at medium range order. The existence of a strong peak in the RDF at 5 Å, the nature of which has been fully understood, is of particular interest since it allows us to determine the site occupancy[2] of solute atoms in the ternary dilute alloys. On the one hand, we wish to emphasize the necessity to record data over a wide *k* range with high-statistical quality to perform a reliable and efficient MS analysis. One must be aware of the importance of this constraint if one is interested in using at best all the information contained in the fine-structure spectra. On the other hand, we have also pointed out that one must employ, in an efficient way, the MS DW factors to reduce the number of varying free parameters during the MS fitting procedure.

Concerning that point, a recently proposed approach[36,37] based on local force constants seems to be promising. Once these two difficulties are overcome, the MS technique should even be more attractive since it should allow us to determine correlation functions for pairs of atoms at rather long distances, and even correlations between triplets.

ACKNOWLEDGMENTS

One of the authors (J.J.R.) thanks the University of Poitiers for hospitality, where part of this work was carried out during a stay as Associate Professor, and the U.S. D.O.E. for support through Grant No. DE-FG03-97ER45623/A000.

*Permanent address: Department of Physics, University of Washington, Seattle, WA 98195–1560.

[1] C. MacCullough, J. J. Valencia, C. G. Levi, and R. Mehrabian, Acta Metall. **37**, 1321 (1989).
[2] M. Jaouen, T. Sikora, G. Hug, and M.G. Walls, J. Phys. IV **10**, 79 (2000).
[3] S. I. Zabinsky, J. J. Rehr, A. L. Ankudinov, R. C. Albers, and M. J. Eller, Phys. Rev. B **52**, 2995 (1995).
[4] G. Hug and E. Fries, in *Gamma Titanium Aluminides*, edited by Y.-W. Kim, D. M. Dimiduk, and M. H. Loretto (Minerals, Metals and Materials Soc., Warrendale, PA, 1999), p. 125.
[5] R. G. Egerton, *Electron Energy Loss Spectroscopy in the Electron Microscope* (Plenum, New York, 1986).
[6] W. Gudat and C. Kunz, Phys. Rev. Lett. **29**, 169 (1972).
[7] J. Mimault, J. J. Faix, T. Girardeau, M. Jaouen, and G. Tourillon, Meas. Sci. Technol. **5**, 482 (1994).
[8] G. Blanche, G. Hug, M. Jaouen, and A.-M. Flank, Ultramicroscopy **50**, 141 (1993).
[9] G. Hug, G. Blanche, M. Jaouen, A.-M. Flank, and J. J. Rehr, Ultramicroscopy **59**, 121 (1995).
[10] J. Wong, G. George, J. Pickering, Z. Rek, M. Rowen, T. Tanaka, G. Via, and G. E. Brown Jr., Solid State Commun. **92**, 559 (1994).
[11] S. L. M. Schroeder, G. D. Moggridges, R. M. Lambert, and T. Rayment, J. Phys. IV **C2 7**, 91 (1997).
[12] A. Erbill, G. S. Cargill III, R. Frahm, and R. F. Boehme, Phys. Rev. B **37**, 2450 (1988).
[13] W. T. Elam, J. P. Kirland, R. A. Neiser, and P. O. Wolf, Phys. Rev. B **38**, 26 (1988).
[14] T. Girardeau, J. Mimault, M. Jaouen, P. Chartier, and G. Tourillon, Phys. Rev. B **46**, 7144 (1992).
[15] W. L. Schaich, Phys. Rev. B **29**, 6513 (1984).
[16] M. Qian, M. Sarikaya, and E. A. Stern, Ultramicroscopy **68**, 163 (1997).
[17] D. Haskel, M. Qian, E. A. Stern, and M. Sarikaya, J. Phys. IV **C2 7**, 577 (1997).
[18] T. Sikora, Ph.D. thesis, Poitiers University, 1997.
[19] D. E. Sayers, E. A. Stern, and F. W. Lytle, Phys. Rev. Lett. **27**, 1024 (1971).
[20] E. A. Stern, Phys. Rev. B **10**, 3027 (1974).
[21] P. A. Lee and J. B. Pendry, Phys. Rev. B **11**, 2795 (1975).
[22] E. A. Stern and W. M. Heald, in *Basic Principles and Applications of EXAFS, Handbook of Synchrotron Radiation* (North-Holland, New York, 1993).
[23] E. A. Stern, in *X-Ray Absorption: Principles, Applications, Techniques of EXAFS, SEXAFS, and XANES*, edited by D. C. Konigsberger and R. Prins (Wiley, New York, 1988).
[24] M. Newville, P. Livins, Y. Yacoby, J. J. Rehr, and E. A. Stern, Phys. Rev. B **47**, 14 136 (1993).
[25] J. J. Rehr, C. H. Booth, F. Bridges, and S. I. Zabinsky, Phys. Rev. B **49**, 12 347 (1994).
[26] M. Newville, B. Ravel, D. Haskel, J. J. Rehr, E. A. Stern, and Y. Yacoby, Physica B **208/209**, 154 (1995).
[27] M. Vaarkamp, I. Dring, R. J. Oldham, E. A. Stern, and D. C. Koningsberger, Phys. Rev. B **50**, 7872 (1994).
[28] A. I. Ankudinov and J. J. Rehr, J. Phys. IV **C2 7**, 121 (1997).
[29] L. Hedin and S. Lundquist, *Solid State Physics: Advances in Research and Applications* (Academic, New York, 1969), Vol. 23.
[30] E. Sevillano, H. Meuth, and J. J. Rehr, Phys. Rev. B **20**, 4908 (1979).
[31] I. Phan-Courson, Ph.D. thesis, University of Paris VI, 1993.
[32] J. C. H. Spence and J. Taftø, J. Microsc. **230**, 147 (1982).
[33] A. Loiseau, Thèse de Doctorat d'Etat, University of Paris VI, 1985.
[34] J. Max, *Méthodes et Techniques de Traitement du Signal et Applications aux Mesures Physiques* (Masson, Paris, 1971).
[35] T. Sikora, M. Jaouen, and G. Hug, Philos. Mag. A **79**, 2157 (1999).
[36] A. V. Poiarkova and J. J. Rehr, Phys. Rev. B **59**, 948 (1999).
[37] A. V. Poiarkova and J. J. Rehr, J. Synchrotron Radiat. **6**, 313 (1999).